

# Diverging evolution of light pollution indicators: can the Globe at Night and VIIRS-DNB measurements be reconciled?

Salvador Bará<sup>1,\*</sup>, and José J. Castro-Torres<sup>2</sup>

<sup>1</sup> *Independent scholar. Former profesor titular (retired) at Universidade de Santiago de Compostela (USC), Santiago de Compostela, 15782 Galicia (Spain, European Union)*

<sup>2</sup> *Laboratory of Vision Sciences and Applications, Department of Optics, University of Granada, Granada, 18071 (Spain, European Union)*

\* Corresponding author. e-mail: salva.bara@usc.gal

---

**Abstract:** The radiance of nighttime artificial lights measured by the VIIRS-DNB instrument on board the satellite Suomi-NPP increases at an average rate  $\sim 2.2$  %/yr worldwide, whereas the artificial radiance of the night sky deduced from the Globe at Night (GAN) unaided-eye observations of the number of visible stars is reported to increase at an average rate  $\sim 9.6$  %/yr. The difference between these two estimates is remarkable. This raises the question of whether the diverging temporal evolution of these indicators could be due to changes in the spectral composition of outdoor artificial light, consequence of the current process of replacement of lighting technologies. This paper presents a model for evaluating the temporal rate of change of different light pollution indicators and applies it to the VIIRS-DNB vs GAN issue, based on available data. The results show that the reported difference could be explained by spectral changes alone, if the visual observations are made under scotopic adaptation in some specific transition conditions. In case of photopic adapted observers, however, reconciling these two measurement sets requires the existence of additional light sources that affect the Globe at Night observations but do not show up in the VIIRS-DNB data. The lumen emissions of these specific sources should increase at a rate 6 %/yr worldwide, adding to the estimated 3 %/yr of the remaining lights deduced from the VIIRS-DNB measurements corrected for spectral shift.

---

**Keywords:** light pollution ; glare ; Globe at Night ; VIIRS-DNB; global change

## 1. Introduction

The temporal evolution of light pollution indicators provides useful information about the progression and extent of the unwanted effects of artificial light at night. Light pollution indicators are observable quantities derived from the spectral radiance of the anthropogenic light [1-4]. They can be linear or non-linear, depending on their definition in terms of the radiance at the observer location [5,6]. They can be applied to the light received directly from

the sources, to the light scattered by small-scale inhomogeneities of the material medium through which light propagates (e.g. the atmosphere or the water column), or to a combination of both.

Light pollution indicators are evaluated in different spectral bands, depending on the effects under study and the available measurement devices. Common detection bands include, among others, the human photopic and scotopic spectral luminous efficiencies [7,8], the five human photoreceptor alfa-opic curves [9-11], various sets of classical astronomical filters [12] including the RGB system [13-15], satellite [16,17] and ground-based [18,19] radiometer passbands, and a wide range of animal photoreceptor sensitivities and action spectra [20].

Light pollution indicators may also provide valuable insights about the evolution of the global amount of artificial light emissions. The rationale is that the radiance measured at the observer location depends linearly on the weighted emissions of the sources, mediated by the state of the atmosphere [2,5,21,22]. It has long been known, however, that the time evolution of different indicators, even if correlated, may differ in magnitude and sign. The same change in the number and types of artificial light sources and/or in their geographical distribution around the observer may result in increasing values for some indicators and decreasing values for others. A situation of this kind usually arises when there is a shift in the spectral composition of the light and the indicators are evaluated in different spectral bands [23,24]. While the evolution of each individual indicator provides information about the changes in the specific effect it measures (which may well be different from one indicator to another), their divergent collective behavior can be a problem when it comes to using them as a proxy to assess other quantities of interest as e.g. the evolution of the global amount of artificial light emissions.

An interesting case of diverging temporal evolution has been recently reported [25]. According to these results, the artificial night sky brightness derived from the Globe at Night unaided-eye star-counting citizen science campaigns increased at an average rate  $9.6 \pm 0.4$  %/yr during the period 2011-2022, substantially faster than the estimated  $\sim 2.2$  %/yr average rate of increase of the overall artificial light emissions derived from the VIIRS-DNB band satellite radiance measurements in the period 2012-2016 [26].

Can these results be reconciled? If so, what can they teach us about the processes at play? Recall that, everything else being constant (average state of the atmosphere, spatial distribution, and spectral and angular emission patterns of the ensemble of light sources), one would expect that the rate of change of the artificial night sky brightness should be equal to the rate of change of the total (distance-weighted) light emissions in the territory surrounding the observer, irrespective from the spectral sensitivity bands in which each indicator is measured. Different rates of change could arise, however, if either the average state of the atmosphere, the characteristics of the sources (spatial distribution and spectral and angular emission patterns), or a combination of these factors, would actually change in time.

This paper describes a simplified model for analyzing these situations, derived from first principles of light pollution propagation. This approach is applied to interpret the seemingly divergent results from Globe at Night observations [25] and VIIRS-DNB satellite nighttime measurements [26]. The goal is to assess whether their different evolution rates can be

explained by the change of spectrum of artificial light associated with the current transition from low CCT high-pressure sodium lamps to high CCT LED sources, or other additional factors are required to fully explain them.

## 2. Time evolution of light pollution indicators

The two light pollution indicators analyzed in this paper are (i) the artificial radiance of the night sky,  $L_{\text{GAN}}(t)$ , estimated from multiple unaided-eye observations of the number of visible stars on selected regions of the sky, made by Globe at Night citizen scientists in a wide set of locations worldwide, and (ii) the top-of-atmosphere radiance of nighttime artificial lights,  $L_{\text{DNB}}(t)$ , measured by the VIIRS radiometer onboard the Suomi-NPP satellite in its day-night band (DNB). The basic equations for their time evolution are described in this section.

From a formal standpoint both indicators are angular field-of-view averages of spectral radiances integrated within their respective sensitivity bands. The angular averaging for  $L_{\text{GAN}}(t)$  is made over the solid angle span of the selected sky region (typically a well-known constellation or asterism), being the spectral integration carried out within the human photopic band. The corresponding luminance of the sky, in  $\text{cd}\cdot\text{m}^{-2}$ , can be obtained by multiplying the radiance  $L_{\text{GAN}}(t)$  in  $\text{W}\cdot\text{m}^{-2}\cdot\text{sr}^{-1}$  by the luminous efficacy of radiation  $K_r = 683 \text{ lm}\cdot\text{W}^{-1}$ . The angular averaging for  $L_{\text{DNB}}(t)$ , in turn, is carried out within each pixel ( $15\times 15$  arcsecond-square) of the satellite image, being the spectral integration made in the DNB sensitivity band. For the sake of definiteness, the following equations will generically refer to the indicators as 'radiances', although all expressions in this section could equally be applied to any other linear indicator (e.g. horizontal irradiances or illuminances) by substituting the appropriate quantities.

Any linear light pollution indicator can be expressed in terms of the basic properties of the sources and the environment. A formal, step-by-step derivation of this relationship may be found in Ref. [5]. For the purposes of this paper it is convenient to express the radiances  $L_{\beta}(t)$ ,  $\beta \in \{\text{GAN}, \text{DNB}\}$ , as a weighted sum over wavelengths  $\lambda$ :

$$L_{\beta}(t) = \int_{\lambda} F_{\beta}(\lambda, t) E(\lambda, t) d\lambda \quad (1)$$

where  $L_{\beta}(t)$  has dimensions  $\text{W}\cdot\text{m}^{-2}\cdot\text{sr}^{-1}$ ,  $t$  is the time, and  $E(\lambda, t)$  is the average spectral radiant flux emitted per unit area by the artificial light sources in the relevant patch of territory surrounding the observer, expressed in  $\text{W}\cdot\text{m}^{-2}\cdot\text{nm}^{-1}$ .  $E(\lambda, t)$  refers to the flux emitted by all sources (luminaires, windows, self-luminous billboards...), which in present-day installations is mostly sent towards the surrounding surfaces (pavements, façades, grasslands,...) and, in a smaller proportion, directly towards the upper hemisphere.

The function  $F_{\beta}(\lambda, t)$  in Eq. (1) has dimensions  $\text{sr}^{-1}$  and it accounts for the physical processes that take place along the light propagation path, since the light leaves the sources until it is detected. It can be formally defined as the spectral radiance at the observer location,

weighted by the spectral sensitivity of the  $\beta$ -band, produced by a unit of spectral radiant flux  $E(\lambda, t)$  of the sources.

$F_\beta(\lambda, t)$  depends on the particular emission-propagation-detection configuration. It generally contains the result of many intermediate operations, often including path integrals and spatial and angular integrations over the sources' spatial distribution and angular emission patterns, respectively. It takes into account the optical properties of the surfaces with which the light interacts (bidirectional reflectance distribution functions) and the state of the atmosphere through which it propagates, which jointly determine the absorption and scattering of light from the source to the detector. Their specific values have to be calculated for each indicator and will be discussed in section 3. The detailed form of  $F_\beta(\lambda, t)$ , however, is not required for the present section.

To obtain the time evolution equations, let us assume that the ensemble of lamps is composed by sources of  $k = 1, \dots, S$  different technologies (HPS, LED of various CCT, etc), whose nominal spectral radiant fluxes, normalized to one lm, are  $\hat{\Phi}_k(\lambda)$ . The spectral flux emitted per unit area of the territory  $E(\lambda, t)$  can then be expressed as:

$$E(\lambda, t) = \sum_{k=1}^S N_k(t) \hat{\Phi}_k(\lambda) = N(t) \sum_{k=1}^S \gamma_k(t) \hat{\Phi}_k(\lambda) \quad (2)$$

where  $N_k(t)$  is the amount of lumen per unit area emitted by the  $s$ -th type of lamps,  $N(t) = \sum_{k=1}^S N_k(t)$  is the total lumen emitted per unit area, and  $\gamma_k(t) = N_k(t)/N(t)$  is the fractional contribution of the  $s$ -th type of lamps, being  $\sum_{k=1}^S \gamma_k(t) = 1$ . The dimensions of  $\hat{\Phi}_k(\lambda)$  are  $\text{W} \cdot \text{m}^{-2} \cdot \text{nm}^{-1} / (\text{lm} \cdot \text{m}^{-2}) = \text{W} \cdot \text{nm}^{-1} \cdot \text{lm}^{-1}$ .

From Eqs. (1) and (2), we have

$$L_\beta(t) = N(t) \sum_{k=1}^S \gamma_k(t) \mathcal{H}_{\beta k}(t) \quad (3)$$

where

$$\mathcal{H}_{\beta k}(t) \equiv \int_{\square} F_\beta(\lambda, t) \hat{\Phi}_k(\lambda) d\lambda \quad (4)$$

are terms which depend on the spectra of the sources, the physics of light propagation, and the detection band, but not on the amount of lumen emitted per unit area,  $N(t)$ , nor on their allocation among several types of lighting technologies,  $\gamma_k(t)$ . The dimensions of  $\mathcal{H}_{\beta k}(t)$  are, from Eq. (3),  $\text{W} \cdot \text{m}^{-2} \cdot \text{sr}^{-1} / (\text{lm} \cdot \text{m}^{-2})$ . They can be understood as the radiance detected in the  $\beta$ -band per  $\text{lm} \cdot \text{m}^{-2}$  emitted by the  $k$ -th type of sources.

We are primarily interested in the evolution of the indicators due to changes in the spectral composition of the light via  $\gamma_k(t)$  and changes in the total amount of emissions via  $N(t)$ , so we will analyze here the case in which the  $\mathcal{H}_{\beta k}$  factors do not depend on time. Denoting by a dot

above any variable its derivative with respect to time,  $\dot{x} \equiv dx/dt$ , the absolute rate of change of the radiance  $L_\beta(t)$  is:

$$\dot{L}_\beta(t) = \sum_{k=1}^S [\dot{N}(t) \gamma_k(t) + N(t) \dot{\gamma}_k(t)] \mathcal{H}_{\beta k} \quad (5)$$

The relative rate of change is then given by

$$\frac{\dot{L}_\beta(t)}{L_\beta(t)} = \dot{n}(t) + \frac{\sum_{k=1}^S \dot{\gamma}_k(t) \mathcal{H}_{\beta k}}{\sum_{k=1}^S \gamma_k(t) \mathcal{H}_{\beta k}} \quad (6)$$

where  $\dot{n}(t) \equiv \dot{N}(t)/N(t)$  is the relative rate of change of the total lumen emissions per unit area, and the second term of the right-hand side of Eq. (6) accounts for the relative change in the spectral composition of the emitted light. All terms in Eq. (6) can be expressed in units  $\text{yr}^{-1}$  or equivalently in  $\%/ \text{yr}$ .

The above formulation can be applied to a transition process in which an initial population of high-pressure sodium lamps is progressively replaced by 4000 K LED lamps, with normalized spectra  $\hat{\Phi}_{\text{HPS}}(\lambda)$  and  $\hat{\Phi}_{\text{LED}}(\lambda)$ . The  $\mathcal{H}_{\beta k}$  factors are denoted as  $\mathcal{H}_{\beta, \text{HPS}}$  and  $\mathcal{H}_{\beta, \text{LED}}$ , and the fractional contributions are  $\gamma_{\text{HPS}}(t)$  and  $\gamma_{\text{LED}}(t)$ , verifying  $\gamma_{\text{LED}}(t) = 1 - \gamma_{\text{HPS}}(t) \equiv \gamma(t)$ ,  $\gamma_{\text{HPS}}(t) = 1 - \gamma(t)$  respectively. For this transition,

$$L_\beta(t) = N(t) \{ [1 - \gamma(t)] \mathcal{H}_{\beta, \text{HPS}} + \gamma(t) \mathcal{H}_{\beta, \text{LED}} \} \quad (7)$$

and, finally,

$$\frac{\dot{L}_\beta(t)}{L_\beta(t)} = \dot{n}(t) + \frac{\left( \frac{\mathcal{H}_{\beta, \text{LED}}}{\mathcal{H}_{\beta, \text{HPS}}} - 1 \right) \dot{\gamma}(t)}{1 + \left( \frac{\mathcal{H}_{\beta, \text{LED}}}{\mathcal{H}_{\beta, \text{HPS}}} - 1 \right) \gamma(t)} \quad (8)$$

### 3. Expected evolution of VIIRS-DNB versus visual radiances

The reported DNB and GAN radiance rates are  $\dot{L}_{\text{DNB}}(t)/L_{\text{DNB}}(t) = 2.2 \%/ \text{yr}$  [26] and  $\dot{L}_{\text{GAN}}(t)/L_{\text{GAN}}(t) = 9.6 \%/ \text{yr}$  [25], respectively. In order to elucidate if these diverging rates may be explained by a combination of the spectral shift due to the change from HPS to LED and the evolution of the overall emissions affecting both indicators, the numerical ratios  $\mathcal{H}_{\text{DNB,LED}}/\mathcal{H}_{\text{DNB,HPS}}$  and  $\mathcal{H}_{\text{GAN,LED}}/\mathcal{H}_{\text{GAN,HPS}}$  to be used in Eq. (8) shall be estimated.

Some of these ratios are already available in the literature. Recall that for an initial condition  $\gamma(t_0) = 0$ , in which all lamps are HPS at  $t = t_0$ , and a final condition  $\gamma(t_1) = 1$ , in which all lamps are LED at  $t = t_1$ , we have, from Eq. (7),

$$\frac{L_\beta(t_1)}{L_\beta(t_0)} = \frac{N(t_1)}{N(t_0)} \times \frac{\mathcal{H}_{\beta, \text{LED}}}{\mathcal{H}_{\beta, \text{HPS}}} \quad (9)$$

so that the required ratios  $\mathcal{H}_{\beta,LED}/\mathcal{H}_{\beta,HPS}$  may be obtained as the ratios of radiances at the start and the end of the transition period,  $L_{\beta}(t_1)/L_{\beta}(t_0)$ , calculated for constant lumen emissions  $N(t_1) = N(t_0)$ .

The values of the VIIRS-DNB  $\mathcal{H}_{\beta k}$  terms for a standard configuration of the sources, atmosphere and observation geometry in a transition from HPS to 4000 K LED were calculated in [29]. They were found to be  $\mathcal{H}_{DNB,LED} = 0.081 \times 10^{-3}$  and  $\mathcal{H}_{DNB,HPS} = 0.107 \times 10^{-3}$ , both in  $\text{W}\cdot\text{m}^{-2}\cdot\text{sr}^{-1}/(\text{lm}\cdot\text{m}^{-2})$ . This suggests for the VIIRS-DNB observations a ratio  $\mathcal{H}_{DNB,LED}/\mathcal{H}_{DNB,HPS} \approx 0.76$ .

The visual GAN ratio  $\mathcal{H}_{GAN,LED}/\mathcal{H}_{GAN,HPS}$  arises from two contributions, both related to the scattering of artificial light. Recall that GAN radiances are estimated from unaided-eye observations of the artificial sky brightness, using as a proxy the number of visible stars. This number is limited by the scattered artificial light reaching the retina, which reduces the luminance contrast of the stars against the polluted sky background. As the sky luminance increases, the dimmer stars progressively fall below the luminance contrast threshold of the observer and the number of visible stars decreases. Two main scattering processes have to be taken into account: the scattering of light in the terrestrial atmosphere (ATM) and the scattering within the observer eye (IOC) [28]. Both contribute to the build-up of the anthropogenic luminance perceived by the sky observers in light polluted places.

From Eqs. (1)-(4) we have

$$\frac{\mathcal{H}_{GAN,LED}}{\mathcal{H}_{GAN,HPS}} = \frac{\mathcal{H}_{GAN,LED}^{ATM} + \mathcal{H}_{GAN,LED}^{IOC}}{\mathcal{H}_{GAN,HPS}^{ATM} + \mathcal{H}_{GAN,HPS}^{IOC}} \quad (10)$$

The relative contribution of the ATM and IOC scattering terms to the perceived sky luminance depends on multiple factors, including the spatial distribution of the light sources around the observer, their angular emission patterns and spectra, the reflective properties of the surrounding surfaces, the direction of the line of sight, the total lumen emissions and the adaptation state of the observer. At short distances from the luminaires ( $\sim 10\text{-}20$  m) the intraocular scattering radiance  $L_{GAN}^{IOC}(t)$  due to nearby lamps can be larger than or equal to the zenith radiance  $L_{GAN}^{ATM}(t)$  due to the atmospheric scattering of the ensemble of urban emissions, while at medium to long distances from the nearest luminaire the atmospheric scattering is the leading term [28]. Eq. (10) can be rewritten in a more convenient form, in terms of the ratio of intraocular and atmospheric scattered radiances at the initial time,  $c \equiv L_{GAN}^{IOC}(t_0)/L_{GAN}^{ATM}(t_0)$ . From our assumed initial conditions ( $\gamma(t_0) = 0$ , all lamps HPS), it follows  $c = \mathcal{H}_{GAN,HPS}^{IOC}/\mathcal{H}_{GAN,HPS}^{ATM}$  and Eq. (10) has the equivalent form:

$$\frac{\mathcal{H}_{GAN,LED}}{\mathcal{H}_{GAN,HPS}} = \frac{1}{(1+c)} \left( \frac{\mathcal{H}_{GAN,LED}^{ATM}}{\mathcal{H}_{GAN,HPS}^{ATM}} + c \frac{\mathcal{H}_{GAN,LED}^{IOC}}{\mathcal{H}_{GAN,HPS}^{IOC}} \right) \quad (11)$$

Equation (11) allows treating separately the effects of the atmospheric and the intraocular processes by using their own ratios  $\mathcal{H}_{GAN,LED}^{ATM}/\mathcal{H}_{GAN,HPS}^{ATM}$  and  $\mathcal{H}_{GAN,LED}^{IOC}/\mathcal{H}_{GAN,HPS}^{IOC}$ .

The parameter space of this problem is exceedingly large and it seems not feasible to analyze all possible source and observer configurations relevant for GAN observations. However, some estimations can be made for reasonable conditions of observation.

The evolution of the artificial radiance  $L_{\text{GAN}}^{\text{ATM}}(t)$  of the zenith night sky for the transition HPS to 4000 K LED has been analyzed in [24]. Recall that the ratio  $\mathcal{H}_{\text{GAN,LED}}^{\text{ATM}}/\mathcal{H}_{\text{GAN,HPS}}^{\text{ATM}}$  is equal to the value of  $L_{\text{GAN}}^{\text{ATM}}(t_1)/L_{\text{GAN}}^{\text{ATM}}(t_0)$  for constant lumen emissions ( $N(t_1)/N(t_0) = 1$ ) and  $\mathcal{H}_{\text{GAN},k}^{\text{ATM}}$  terms independent of time. This situation corresponds to the top-left panel of Figure 6 of [24]. The  $L_{\text{GAN}}^{\text{ATM}}(t_1)/L_{\text{GAN}}^{\text{ATM}}(t_0)$  photopic value for a distance source-observer 0.1 km, and the scotopic ones for several distances can be deduced from the value of the curves in that Figure for the abscissa equal to 1 (all lamps LED,  $\gamma = 1$ ). The normalized radiances  $L_{\text{GAN}}^{\text{ATM}}(t)/L_{\text{GAN}}^{\text{ATM}}(t_0)$  are expressed in the vertical axis of that plot as astronomical magnitude changes  $\Delta m(t)$  with respect to the initial conditions, so that  $L_{\text{GAN}}^{\text{ATM}}(t)/L_{\text{GAN}}^{\text{ATM}}(t_0) = 10^{-0.4 \times \Delta m(t)}$ . The values of  $\mathcal{H}_{\text{GAN,LED}}^{\text{ATM}}/\mathcal{H}_{\text{GAN,HPS}}^{\text{ATM}}$  computed here for several distances source-observer in the photopic and scotopic bands are listed in Table 1 below.

**Table 1.** Values of  $\mathcal{H}_{\text{GAN,LED}}^{\text{ATM}}/\mathcal{H}_{\text{GAN,HPS}}^{\text{ATM}}$  for the atmospheric scattering term [24]

Distance source- observer (km)	$\mathcal{H}_{\text{GAN,LED}}^{\text{ATM}}/\mathcal{H}_{\text{GAN,HPS}}^{\text{ATM}}$ (photopic)	$\mathcal{H}_{\text{GAN,LED}}^{\text{ATM}}/\mathcal{H}_{\text{GAN,HPS}}^{\text{ATM}}$ (scotopic)
0.1	1.062	2.811
0.5	1.061	2.805
1.0	1.060	2.802
5.0	1.059	2.787
10	1.055	2.771
50	1.023	2.663
100	0.991	2.553

**Table 2.** Values of  $\mathcal{H}_{\text{GAN,LED}}^{\text{IOC}}/\mathcal{H}_{\text{GAN,HPS}}^{\text{IOC}}$  for the intraocular scattering term [see Appendix]

Observer group	$\mathcal{H}_{\text{GAN,LED}}^{\text{IOC}}/\mathcal{H}_{\text{GAN,HPS}}^{\text{IOC}}$ (photopic)	$\mathcal{H}_{\text{GAN,LED}}^{\text{IOC}}/\mathcal{H}_{\text{GAN,HPS}}^{\text{IOC}}$ (scotopic)
> 40 yr	1.031	2.799
Blue-eyed	1.008	2.713
Green and light brown-eyed	1.013	2.758
Brown-eyed	1.097	2.915
Dark brown-eyed	1.133	2.965

The evolution of the artificial radiance term of intraocular scattering,  $L_{\text{GAN}}^{\text{IOC}}(t)$ , may be studied by means of the glare point spread function [28-30]. A formulation based on the spectral straylight parameter  $s(\lambda)$  is described in the Appendix, enabling the analysis of the effects

derived from changing the spectra of the light sources. The strength and the spectral behavior of the intraocular scattering term depend on the demographics of the observer population [29-30]. The spectral  $s(\lambda)$  functions used in this work for different populations are based on the discrete sets of narrowband measurements reported by Coppens et al. [31] for each group of observers, at wavelengths 457, 503, 548, 583 and 625 nm. For the purposes of the present calculations, the Coppens et al. values for each observer group were linearly interpolated within the data range, and linearly extrapolated to cover the remaining part of the visible region of the spectrum below 457 nm and above 625 nm. The Coppens et al. populations are defined by age (>40 yr old) or eye color and pigmentation (blue, green and light-brown, brown, and dark-brown eyes). The resulting  $\mathcal{H}_{\text{GAN,LED}}^{\text{IOC}}/\mathcal{H}_{\text{GAN,HPS}}^{\text{IOC}}$  ratios for each observer group in the photopic and scotopic bands are listed in Table 2. These ratios are consistently larger than 1, and larger for scotopic than for photopic observers, reflecting the fact that high CCT LED give rise to more intense glare effects due to their high blue component. The smallest values of these ratios correspond to weakly pigmented eyes (blue eyes), for which the short wavelength scattering of the iris, cornea and eye lens is partially balanced by the long-wavelength scattering from the highly vascularized retina [29-30].

Finally, the contributions of the ATM and IOC processes were combined according to Eq. (11) with  $c = 1$  (equal contribution of both processes under HPS illumination).

In order to apply Eq. (8) to our present problem, it is necessary to estimate the form of the function  $\gamma(t)$  and calculate its time derivative,  $\dot{\gamma}(t)$ . Recall that in a two-source transition process  $\gamma(t)$  is the ratio of the lumen per unit area emitted by the new sources (in our case, LED) to the total ones (LED+HPS). Its time derivative is the rate of substitution of old by new lamps, on a lumen per lumen basis. This rate is not precisely known due to the lack of systematic lamp inventory updates, but it is expected to vary widely from one region of the world to another. To get some insight about the order of magnitude of its effects, we assume here a linear evolution at a constant time rate along a period of  $T_0$  years, such that  $\gamma(t) = t/T_0$  and  $\dot{\gamma}(t) = 1/T_0$  (expressed in 1/yr or %/yr). The calculations in this section are made for three scenarios,  $T_0 = 10, 20$ , and 30 years, corresponding to substitution rates  $\dot{\gamma}(t) = 10 \text{ \%/yr}$ ,  $5 \text{ \%/yr}$  and  $(10/3) \text{ \%/yr}$ , respectively, relative to the total (and constant) number of emitted lumen.

The results of the calculations with these parameters for the VIIRS-DNB and GAN observations (photopic and scotopic adapted observers) are shown in Fig. 1. The vertical axis shows the rates of change of the radiance, expressed in % per year, for the normalized time  $t/T_0$  displayed in the horizontal axis. The lines labelled 'Measured' correspond to the reported values  $\dot{L}_{\text{DNB}}(t)/L_{\text{DNB}}(t) = 2.2 \text{ \%/yr}$  [26] and  $\dot{L}_{\text{GAN}}(t)/L_{\text{GAN}}(t) = 9.6 \pm 0.4 \text{ \%/yr}$  [25]. The lines labeled with  $T_0$  periods in years correspond to the calculated values of the second term of the right-hand side of Eq. (8), that is, the change rates associated with the spectral shift of the sources. The differences between the measured and the calculated spectral quantities are the estimated rates of change of the total emissions in lumen per unit area,  $\dot{n}(t)$ , in %/yr.



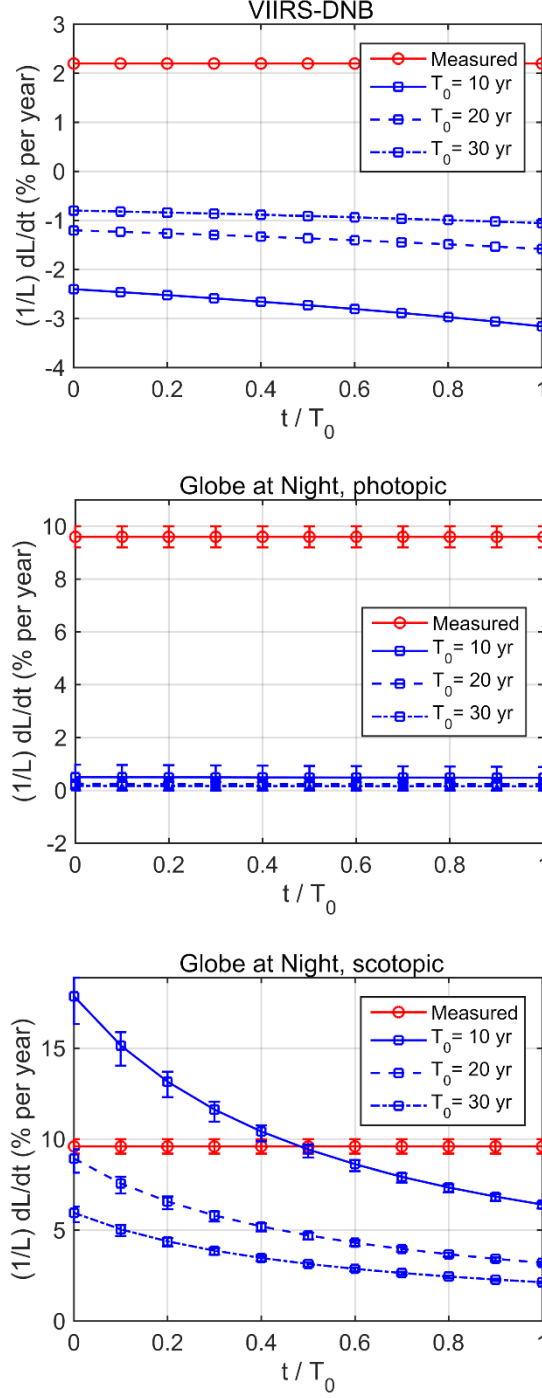


**Fig. 1.** Radiance change rates  $\dot{L}_\beta(t)/L_\beta(t)$ , in % per year, vs. normalized time  $t/T_0$  for (*top*) VIIRS-DNB data, (*middle*) GAN observations assuming photopic adaptation of the observers and (*bottom*) GAN under scotopic adaptation of the observers. The constant values labeled 'Measured' correspond to the reported rates 2.2 %/yr for DNB and  $9.6 \pm 0.4$  %/yr for GAN. Lines labeled with  $T_0$  in years display the second term of the right-hand side of Eq. (8), that is, the radiance change rates associated with the spectral shift HPS to LED at constant lumen emissions, calculated for the average of the values of  $\mathcal{H}_{\text{GAN,LED}}^{\text{ATM}}/\mathcal{H}_{\text{GAN,HPS}}^{\text{ATM}}$  and  $\mathcal{H}_{\text{GAN,LED}}^{\text{ATM}}/\mathcal{H}_{\text{GAN,HPS}}^{\text{ATM}}$  for each observer adaptation state listed in Tables 1 and 2, combined with a factor  $c = 1$  in Eq. (11). The distances between the measured values and these lines are the estimated rates of change of the lumen emissions

per unit area,  $\dot{n}(t)$ , in %/yr. The bars above and below of the symbols mark the rates obtained using the maximum and minimum values of each column of Tables 1 and 2.

As expected and previously reported [24,27], the VIIRS-DNB radiance rates associated with the spectral change from HPS to 4000 K LED, at constant emitted lumen, are negative. This is due, among other things, to the progressive reduction of the contribution of the HPS 819 nm near-infrared line and the inability of the DNB band to detect the emissions of the 450 nm blue peak of phosphor-coated LED. Fig. 1(a) suggests that the DNB data are compatible with an overall emission change  $\dot{n}_{\text{DNB}}(t) \approx 3$  %/yr, for an intermediate value  $T_0 = 20$  yr ( $\dot{\gamma}(t) = 5$  %/year). The situation is substantially different for the visual GAN estimates, particularly in the photopic range, for which  $\dot{n}_{\text{GAN,phot}}(t) \approx 9$  %/yr. Assuming that the rate deduced from the VIIRS-DNB data corresponds to the emissions responsible for the global atmospheric scattering (ATM) affecting the GAN observers, the difference of about  $\sim 6$  %/yr should correspond to the increase in the lumen per unit area emissions directly affecting the glare component (IOC) of the GAN visual observations, that is, nearby urban sources that are more efficient to dazzle the GAN observers than to be detected by the VIIRS-DNB. The DNB rate  $\dot{n}_{\text{DNB}}(t) \approx 3$  %/yr is however compatible with the scotopic  $\dot{n}_{\text{GAN,scot}}(t)$  for  $T_0 = 20$  yr and  $\gamma(t) \approx 0.2$ , i.e., at  $t \approx 4$  yr elapsed since the start of the HPS to LED transformation process.

#### 4. Discussion

The results in Section 3 show that the mere change of spectrum in the transition HPS to 4000 K LED, plus the  $\sim 3$  %/yr increase of the overall emissions deduced from the VIIRS-DNB data (corrected for spectral shift), are not enough by themselves to explain the diverging evolution rates of the VIIRS-DNB and the photopic GAN radiances. To reconcile these two sets of observations an additional emissions increase of about  $\sim 6$  %/yr should affect the photopic GAN observations.

This additional increase of emissions, affecting the photopic GAN observations but not the VIIRS-DNB ones, could be attributed to several processes. An obvious candidate would be an increase in the amount of ornamental, commercial, vehicle and advertising lights, including high-luminance LED billboards located in the immediate vicinity of the observer, which are strongly detrimental for star watching. These sources are usually switched on during the first half of the night, a typical time period for unaided-eye GAN observations, and switched off or considerably dimmed in many places at midnight, much earlier than the usual time of VIIRS-DNB data acquisition ( $\sim 01:30$  solar local time). These sources, especially if blocked by local obstacles, could make a small contribution to the total urban light emissions in near-zenith directions within the pixels of mid-resolution satellites (a few hundred meter wide), but could increase substantially the scattered radiance in the first meters of the local air column [32] and inside the observer eye if the lamps are directly visible [28], leading to progressively larger equivalent veiling luminances and corresponding loss of star visibility. Intraocular scattering has an important influence on the perception of sky brightness and star detection in observations close to light sources (such as street lamps) [28], since it is widely known that as

intraocular scattering increases, certain visual functions such as contrast sensitivity or visual discrimination ability are impaired [33]. In addition, intraocular scattering is wavelength dependent, so that for several observer populations there is a greater contribution of intraocular scattering for short wavelengths as other authors have shown [31]. The LED sources that are replacing high-pressure sodium lamps have a significant spectral component of short wavelengths, which would contribute to a greater amount of intraocular scattering in these populations. In fact, it has been clinically demonstrated with young observers that straylight increases for short wavelengths and the visual function under low-illumination conditions worsens [34].

Note that what matters here is not the relative amount of these emissions, but their yearly rate of increase. As far as we know, there are no published reports on the rate of increase of the emissions from these types of ground sources, to which the VIIRS-DNB is almost blind. An average rate  $\sim 6\%$ /yr worldwide might seem excessive, based on anecdotal evidence. However, this topic deserves to be further explored. Citizen science campaigns [35] and comprehensive analyses of administrative authorizations for ornamental, commercial and advertising installations could help to settle this relevant issue.

In turn, the VIIRS-DNB and GAN rates for scotopically adapted observers could be compatible under changes of spectra, without the need of additional GAN sources, in certain circumstances (e.g.  $\gamma(t) \approx 0.2$  and  $t \approx 4$  yr). It is debatable whether scotopic adaptation could be acting in a sufficiently large subset of GAN observations, due to the prevailing high illumination levels in populated areas of our planet. The scotopic predictions, Fig. 1(c), are highly dependent on the assumed functional form and values of  $\gamma(t)$  and  $\dot{\gamma}(t)$ . These functions, which inform of the fraction of HPS emissions already substituted by cold white LED (on a lumen-by-lumen basis) at time  $t$ , and of the rate of substitution, in %/year, are very likely highly variable from one world region to another, and reliable statistical data do not appear to be widely available. Reports from individual countries provide some hints about these differences, which arguably also exist at lower territorial aggregation levels. As of 2020, the LED sources represented a 55% of the total streetlights in the UK [36], being the remaining ones HPS and, in smaller quantities, low-pressure sodium, mercury vapor, and other high-intensity discharge lamps. At that time the HPS to LED conversion was progressing at a rate of 3 %/yr. A US report published the same year [37] quoted a cumulative installed fraction of LED lamps in outdoor lighting of 27.2% in 2016 and 51.4% in 2018. Whereas the  $\gamma(t)$  values for 2018 (US) and 2020 (UK) are of the same order of magnitude, the substitution rate per year seems to be substantially larger in the US case. Note that these published data refer to the fractions of lamps, not to the fractions of lumen emitted by each type of technology which is what  $\gamma(t)$  stands for. Settling this interesting issue requires collecting and analyzing finer-grained data on the actual observation conditions, including the luminance adaptation and demographics of the observers, and on the lamp substitution rates (on a lumen-per-lumen basis) at local levels. Besides, information about the state of the atmosphere at the times of observation should also be collected, to reduce the uncertainty derived from the variability of the atmospheric conditions [38].

## 5. Conclusions

This paper describes a model for evaluating the rate of change of different light pollution indicators. It was applied here to analyze the remarkable difference between the reported rate of change of the radiance measured by the VIIRS-DNB instrument on board the Suomi-NPP satellite, which averages to 2.2 %/yr worldwide, and the rate of change of the radiance deduced from the Globe at Night unaided-eye star observations, which averages to 9.6 %/yr globally.

We calculated the effects of the changes in the spectral composition of outdoor lights (modelled as a HPS to 4000 K LED transition) combined with changes in the amount of lumen emitted per unit area in the territories surrounding the observers. The analysis shows that the VIIRS-DNB and GAN observations could be reconciled, assuming photopic adaptation of the observers, if the GAN observations are affected by specific light sources that do not show up in the VIIRS-DNB measurements. The lumen emissions of these GAN-specific sources should increase at a non-negligible rate of  $\sim 6$  %/yr. They would add to the estimated  $\sim 3$  %/yr increase that is present in both measurement approaches. The VIIRS-DNB measurements, however, could be directly compatible with the GAN observations without the need of additional sources, if the latter were made under scotopic adaptation and both the composition of the lighting inventory and the rate of substitution of HPS by LED have the appropriate values. Settling this interesting issue requires gathering more detailed data on the lamp substitution processes in different regions of the world, as well as on the state of the atmosphere and the observer ocular media conditions.

### AI statement

No AI tools were used in this work.

## APPENDIX: Spectrally-resolved glare model

The equivalent glare luminance  $L_{eq}(\theta)$  in  $\text{cd}\cdot\text{m}^{-2}$  produced by intraocular scattering is commonly related to the glaring illuminance  $E_{gl}$  on the eye pupil, in lx, through the glare point spread function  $\Psi(\theta)$ , with units  $\text{sr}^{-1}$ , defined as [29,30]:

$$L_{eq}(\theta) = \Psi(\theta) E_{gl} \quad (A1)$$

where  $\theta$  is the angle between the observer line of sight and the position of the pointlike glaring source in the visual field, usually expressed in degrees (deg).

Several expressions for  $\Psi(\theta)$  can be found in the literature, with increasing levels of complexity as they aim to describe with progressively better accuracy the angular dependence, including factors like the age of the observers and the degree of pigmentation of their ocular

structures [29,30]. For the purposes of this work we will use the simple inverse squared Stiles-Holladay model  $\Psi(\theta) = s \theta^{-2}$ , where  $s$  is the straylight parameter, with dimensions  $\text{deg}^2 \cdot \text{sr}^{-1}$ , which provides information about the strength of the scattering within the eye.

The parameter  $s$  depends on the spectral composition of the pupil glaring illuminance and on the characteristics of the observers. The spectral dependence of  $s$  has been studied by Coppens et al. [31], using narrow-band filters at five discrete wavelengths in the interval 457nm-625nm, and by Castro-Torres et al. [34] in the RGB channels.

Here we provide a general expression of the value of  $s$  for light of arbitrary spectrum. To formalize it, let us denote by  $E_p(\lambda)$  the spectral irradiance produced by the glare source on the eye pupil, in units  $\text{W} \cdot \text{m}^{-2} \cdot \text{nm}^{-1}$ . The pupil glare illuminance due to the irradiance contained in the spectral interval  $[\lambda, \lambda + d\lambda]$  is then  $dE_{gl}(\lambda) = K_r V(\lambda) E_p(\lambda) d\lambda$ , where  $V(\lambda)$  is the photopic spectral sensitivity function of the human visual system [7], and  $K_r = 683 \text{ lm} \cdot \text{W}^{-1}$ . The corresponding equivalent glare luminance at an angle  $\theta$  can be written as  $dL_{eq}(\theta, \lambda) = K_r V(\lambda) L(\theta, \lambda) d\lambda$ , where  $L(\theta, \lambda)$  is the spectral glare radiance, in  $\text{W} \cdot \text{m}^{-2} \cdot \text{sr}^{-1} \cdot \text{nm}^{-1}$ . Both quantities can be related through a spectral glare PSF that in general will depend not only on  $\theta$  but also on  $\lambda$ ,  $\Psi(\theta, \lambda)$ . So we have

$$dL_{eq}(\theta, \lambda) = \Psi(\theta, \lambda) dE_{gl}(\lambda) \quad (A2)$$

from which

$$L(\theta, \lambda) = \Psi(\theta, \lambda) E_p(\lambda) \quad (A3)$$

which is analog to Eq. (A1), but now written in terms of the *spectral* radiances and irradiances, instead of band-integrated luminances and illuminances. The units of  $\Psi(\theta, \lambda)$  are  $\text{sr}^{-1}$ . For most applications of interest it can be assumed that  $\Psi(\theta, \lambda)$  is a separable function, such that

$$\Psi(\theta, \lambda) = s(\lambda) \psi(\theta) \quad (A4)$$

where  $s(\lambda)$  is the spectral straylight factor, determined from measurements made with quasi-monochromatic light, and  $\psi(\theta)$  is a function carrying the angular dependence of glare, e.g.  $\psi(\theta) = \theta^{-2}$  for the simplest Stiles-Holladay model.

From the above results, expressions for the photopic and scotopic equivalent glare luminances can be easily derived. Recalling the definitions of the photopic  $L_{eq}(\theta)$  and  $E_{gl}$  we have

$$L_{eq}(\theta) = K_r \int_{\lambda} V(\lambda) L(\theta, \lambda) d\lambda = K_r \int_{\lambda} V(\lambda) \Psi(\theta, \lambda) E_p(\lambda) d\lambda \quad (A5)$$

$$E_{gl} = K_r \int_{\lambda} V(\lambda) E_p(\lambda) d\lambda \quad (A6)$$

and, from (A1), (A5), (A6),

$$\Psi(\theta) = \frac{\int_{\lambda} V(\lambda) \Psi(\theta, \lambda) E_p(\lambda) d\lambda}{\int_{\lambda} V(\lambda) E_p(\lambda) d\lambda} \quad (A7)$$

By applying the separability assumption for each wavelength, Eq. (A4), we get

$$\Psi(\theta) = \frac{\int_{\lambda} V(\lambda) s(\lambda) E_p(\lambda) d\lambda}{\int_{\lambda} V(\lambda) E_p(\lambda) d\lambda} \psi(\theta) \quad (A8)$$

so that the straylight parameter  $s$  for light of arbitrary spectrum  $E_p(\lambda)$  is given by

$$s = \frac{\int_{\lambda} V(\lambda) s(\lambda) E_p(\lambda) d\lambda}{\int_{\lambda} V(\lambda) E_p(\lambda) d\lambda} \quad (A9)$$

We can adapt this formulation to our present problem by allowing the spectral irradiance on the pupil to change over time,  $E_p(\lambda, t)$ , and defining the glare radiance indicator as  $L_{\text{GAN}}^{\text{IOC}}(t) \equiv L_{\text{eq}}(\theta_0, t)$  for an external glaring source located at an arbitrary angle  $\theta_0$  within the visual field. Then, from Eqs. (A4) and (A5),

$$L_{\text{GAN}}^{\text{IOC}}(t) = K_r \psi(\theta_0) \int_{\lambda} V(\lambda) s(\lambda) E_p(\lambda, t) d\lambda \quad (A10)$$

Since the most intense glare effects are produced by the direct light from the lamps, the spectral glaring irradiance on the eye pupil  $E_p(\lambda, t)$  is proportional to the spectral radiant flux emitted per unit area by the artificial light sources surrounding the observer,  $E(\lambda, t)$ , appearing in Eq. (1). Then we can write  $E_p(\lambda, t) = C \cdot E(\lambda, t)$  in Eq. (A10), where  $C$  is a constant, and, from Eq. (1) we get

$$F_{\beta}(\lambda, t) = F_{\beta}(\lambda) = C K_r \psi(\theta_0) V(\lambda) s(\lambda) \quad (A11)$$

which is independent from time. Hence, from Eq.(4),

$$\mathcal{H}_{\text{GAN},k}^{\text{IOC}} \equiv C K_r \psi(\theta_0) \int_{\lambda} V(\lambda) s(\lambda) \hat{\Phi}_k(\lambda) d\lambda \quad (A12)$$

where  $\hat{\Phi}_k(\lambda)$  is the spectral radiant flux of a lamp of the  $k$ -th type,  $k \in \{\text{HPS}, \text{LED}\}$ , normalized to 1 lm emission. Finally, the ratio  $\mathcal{H}_{\text{GAN,LED}}^{\text{IOC}}/\mathcal{H}_{\text{GAN,HPS}}^{\text{IOC}}$  is given by:

$$\frac{\mathcal{H}_{\text{GAN,LED}}^{\text{IOC}}}{\mathcal{H}_{\text{GAN,HPS}}^{\text{IOC}}} = \frac{\int_{\lambda} V(\lambda) s(\lambda) \hat{\Phi}_{\text{LED}}(\lambda) d\lambda}{\int_{\lambda} V(\lambda) s(\lambda) \hat{\Phi}_{\text{HPS}}(\lambda) d\lambda} \quad (A13)$$

Equations (A10)-(A13), derived for photopic adaptation, can be rewritten for scotopic observers by replacing the photopic efficacy  $K_r$  and the spectral sensitivity function  $V(\lambda)$  by their scotopic counterparts  $K_r' = 1700 \text{ lm} \cdot \text{W}^{-1}$  and  $V'(\lambda)$ , respectively [8].

## References

- [1] Duriscoe, D.M. Photometric indicators of visual night sky quality derived from all-sky brightness maps. *J Quant Spectrosc Radiat Transf* 2016;181:33–45.  
<https://doi.org/10.1016/j.jqsrt.2016.02.022>
- [2] Cinzano P, Falchi F. The propagation of light pollution in the atmosphere. *Mon Not R Astron Soc* 2012;427, 3337–3357. <https://doi.org/10.1111/j.1365-2966.2012.21884.x>
- [3] Falchi F, Bará S. Computing light pollution indicators for environmental assessment. *Nat Sci* 2021;1:e10019. <https://doi.org/10.1002/ntls.10019>
- [4] Falchi F, Ramos F, Bará S, Sanhueza P, Jaque-Arancibia M, Damke G, Cinzano P. Light pollution indicators for all the major astronomical observatories. *Mon Not R Astron Soc* 2023;519(1): 26–33. <https://doi.org/10.1093/mnras/stac2929>
- [5] Falchi F, Bará S. A linear systems approach to protect the night sky: implications for current and future regulations. *R Soc Open Sci* 2020;7:201501. <https://doi.org/10.1098/rsos.201501>
- [6] Bará S, Pérez-Couto X, Falchi F, Kocifaj M, Masana E. Estimating linear radiance indicators from the zenith night-sky brightness: on the Posch ratio for natural and light-polluted skies, *Mon Not R Astron Soc* 2022;512(2):2125–2134, <https://doi.org/10.1093/mnras/stac410>
- [7] CIE – Commision Internationale de l’Éclairage. CIE 1988 2° Spectral Luminous Efficiency Function for Photopic Vision. CIE 86:1990. Vienna: Bureau Central de la CIE; 1990.
- [8] CIE. CIE spectral luminous efficiency for scotopic vision, International Commission on Illumination (CIE), Vienna: Bureau Central de la CIE; 2019. <https://doi.org/10.25039/CIE.DS.gr6w4b5g>
- [9] Lucas RJ, Peirson SN, Berson DM, Brown TM, Cooper HM, Czeisler CA, Figueiro MG, Gamlin PD, Lockley SW, O’Hagan HB, Price LLA, Provencio I, Skene DJ, Brainard GC. Measuring and using light in the melanopsin age. *Trends Neurosci* 2014;37:1–9. <https://doi.org/10.1016/j.tins.2013.10.004>
- [10] CIE. Commission Internationale de l’Eclairage. CIE System for Metrology of Optical Radiation for ipRGC-Influenced Responses to Light. Publication CIE S 026/E:2018. Vienna: Bureau Central de la CIE; 2018. <https://doi.org/10.25039/S026.2018>
- [11] Schlangen LJM, Price LLA. The Lighting Environment, Its Metrology, and Non-visual Responses. *Front Neurol* 2021;12:624861. <https://doi.org/10.3389/fneur.2021.624861>
- [12] Bessell MS. Standard Photometric Systems. *Annu Rev Astron Astrophys* 2005;43:293–336.
- [13] Cardiel N, Zamorano J, Bará S, Sánchez de Miguel A, Cabello C, Gallego J, García L, González R, Izquierdo J, Pascual S, Robles J, Sánchez A, Tapia C. Synthetic RGB photometry of bright stars: definition of the standard photometric system and UCM library of spectrophotometric spectra. *Mon Not R Astron Soc* 2021;504(3):3730–3748. <https://doi.org/10.1093/mnras/stab997>
- [14] Cardiel N, Zamorano J, Carrasco JM, Masana E, Bará S, González R, Izquierdo J, Pascual S, Sánchez de Miguel A. RGB photometric calibration of 15 million Gaia stars, *Mon Not R Astron Soc* 2021;507(1):318–329. <https://doi.org/10.1093/mnras/stab2124>
- [15] Carrasco JM, Cardiel N, Masana E, Zamorano J, Pascual S, Sánchez de Miguel A, González R, Izquierdo J. Photometric Catalogue for Space and Ground Night-Time Remote-Sensing Calibration:

- RGB Synthetic Photometry from Gaia DR3 Spectrophotometry. *Remote Sens* 2023; 15(7):1767. <https://doi.org/10.3390/rs15071767>
- [16] Elvidge CD, Baugh K, M. Zhizhin M, Hsu FC, Ghosh T. VIIRS night-time lights. *Int J Remote Sens* 2017;38(21):5860-5879. <https://doi.org/10.1080/01431161.2017.1342050>
- [17] Román MO, Wang Z, Sun Q, Kalb V, Miller SD, Molthan A, Schultz L, Bell J, et al. NASA's Black Marble nighttime lights product suite. *Remote Sens Environ* 2018;210:113-143. <https://doi.org/10.1016/j.rse.2018.03.017>
- [18] Hänel A, Posch T, Ribas SJ, Aubé M, Duriscoe D, Jechow A, Kollath Z, Lolkema DE, Moore C, Schmidt N, Spoelstra H, Wuchterl G, Kyba CCM. Measuring night sky brightness: methods and challenges. *J Quant Spectrosc Radiat Transf* 2018;205:278-290. <https://doi.org/10.1016/j.jqsrt.2017.09.008>
- [19] Zamorano J, García C, González R, Tapia C, Sánchez de Miguel A, Pascual S, Gallego J, González E, Picazo P, Izquierdo J, et al. STARS4ALL Night Sky Brightness Photometer. *Int J Sustain Light* 2017;35:49-54. <https://doi.org/10.26607/ijsl.v18i0.21>
- [20] Longcore T. A Compendium of Photopigment Peak Sensitivities and Visual Spectral Response Curves of Terrestrial Wildlife to Guide Design of Outdoor Nighttime Lighting. *Basic Appl Ecol* 2023;73:40-50. <https://doi.org/10.1016/j.baae.2023.09.002>
- [21] Bará S, Lima RC, Photons without borders: quantifying light pollution transfer between territories, *Int J Sustain Light* 2018;20(2):51-61. <https://doi.org/10.26607/ijsl.v20i2.87>
- [22] Sánchez de Miguel A, Kyba CCM, Zamorano J, Gallego J, Gaston KJ. The nature of the diffuse light near cities detected in nighttime satellite imagery, *Sci Rep* 2020;10:7829. <https://doi.org/10.1038/s41598-020-64673-2>
- [23] Sánchez de Miguel A, Aubé M, Zamorano J, Kocifaj M, Roby J, Tapia C. Sky Quality Meter measurements in a colour-changing world. *Mon Not R Astron Soc* 2017;467(3):2966-2979. <https://doi.org/10.1093/mnras/stx145>
- [24] Bará S, Rigueiro I, Lima RC. Monitoring transition: expected night sky brightness trends in different photometric bands. *J Quant Spectrosc Radiat Transf* 2019;239:106644. <https://doi.org/10.1016/j.jqsrt.2019.106644>
- [25] Kyba CCM, Altıntas YO, Walker CE, Newhouse M. Citizen scientists report global rapid reductions in the visibility of stars from 2011 to 2022. *Science* 2023;379:265-268. <https://doi.org/10.1126/science.abq7781>
- [26] Kyba CCM, Kuester T, Sánchez de Miguel A, Baugh K, Jechow A, Hölker F, Bennie J, Elvidge CD, Gaston KJ, Guanter L. Artificially lit surface of Earth at night increasing in radiance and extent. *Sci Adv* 2017;3(11):e1701528. <https://doi.org/10.1126/sciadv.1701528>
- [27] Bará S, Bao-Varela C, Lima RC. Quantitative evaluation of outdoor artificial light emissions using low Earth orbit radiometers. *J Quant Spectrosc Radiat Transf* 2023;295:108405. <https://doi.org/10.1016/j.jqsrt.2022.108405>
- [28] Bará S, Bao-Varela C. Skyglow inside your eyes: intraocular scattering and artificial brightness of the night sky. *Int J Sustain Light* 2023;25(1):1-9. <https://doi.org/10.26607/ijsl.v25i01.130>
- [29] van den Berg TJTP, Franssen L, Coppens JE. Ocular Media Clarity and Straylight. In: Darlene A. Dartt, editor. *Encyclopedia of the Eye*, Vol 3. Oxford: Academic Press; 2010. p 173-183.



- [30] van den Berg TJTP, Franssen L, Kruijt B, Coppens JE. History of ocular straylight measurement: A review. *Z Med Phys* 2013;23:6–20. <http://doi.org/10.1016/j.zemedi.2012.10.009>
- [31] Coppens JE, Franssen L, van den Berg TJTP. Wavelength dependence of intraocular straylight. *Exp Eye Res* 2006;82(4):688-692. <https://doi.org/10.1016/j.exer.2005.09.007>
- [32] Bará S, Bao-Varela C, Kocifaj M. Modeling the artificial night sky brightness at short distances from streetlights. *J Quant Spectrosc Radiat Transf* 2023;296:108456. <https://doi.org/10.1016/j.jqsrt.2022.108456>
- [33] Castro-Torres JJ, Martino F, Casares-López M, Ortiz-Peregrina S, Ortiz C. Visual performance after the deterioration of retinal image quality: induced forward scattering using Bangerter foils and fog filters. *Biomed Opt Express* 2021;12(5):2902-2918. <https://doi.org/10.1364/BOE.424715>
- [34] Castro-Torres JJ, Casares-López M, Ortiz-Peregrina S, Martino F, Gómez-Robledo L, Jiménez JR. Effect of the chromaticity of stimuli on night vision disturbances. *Sci Rep* 2024;14:10183. <https://doi.org/10.1038/s41598-024-61069-4>
- [35] Gokus A, Hänel A, Ruby A, Dröge-Rothaar A, Küchly B, Kyba CCM, Fischer D, et al. The Nachlichter app: a citizen science tool for documenting outdoor light sources in public spaces. *Int J Sustain Light* 2023;25(1):24-59. <https://doi.org/10.26607/ijsl.v25i1.133>
- [36] UK Roads Liaison Group. "State of the Nation: 2020 street lighting report". Chartered Institute of Highways and Transportation, UK Lighting & Technology Board, Streetlighting Advisory Services. January 2021. Available online at <https://ukrlg.ciht.org.uk/media/12713/sotn-report.pdf> [Last accessed 16 September 2024]
- [37] US Department of Energy. "Adoption of Light-Emitting Diodes in Common Lighting Applications". August 2020. Available online at <https://www.energy.gov/eere/ssl/articles/2020-led-adoption-report> [Last accessed 16 September 2024]
- [38] Bará S. Detecting changes in anthropogenic light emissions: limits due to atmospheric variability. *J Quant Spectrosc Radiat Transf* 2024;329:109187. <https://doi.org/10.1016/j.jqsrt.2024.109187>